Mathematical Biosciences and Engineering

MBE, 17(6): 7980–7993.
DOI: 10.3934/mbe.2020405
Received: 05 October 2020
Accepted: 05 November 2020
Published: 11 November 2020

http://www.aimspress.com/journal/MBE

Research article

Two-compartment mathematical modeling in RF tumor ablation: New insight when irreversible changes in electrical conductivity are considered

Dora Luz Castro-López [1], Macarena Trujillo [2], Enrique Berjano [3] and Ricardo Romero-Mendez [1,*]

[1] Facultad de Ingeniería, Universidad Autónoma de San Luis Potosí, San Luis Potosí, SLP 78290, México
[2] BioMIT, Department of Applied Mathematics, Universitat Politècnica de València, Valencia 46022, Spain
[3] BioMIT, Department of Electronic Engineering, Universitat Politècnica de València, Valencia 46022, Spain

*** Correspondence:** Email: rromerom@uaslp.mx.

Abstract: The objective was to explore variations of temperature distribution and coagulation zone size computed by a two-compartment radiofrequency ablation (RFA) model when including simultaneously reversible changes in the tissue electrical conductivity (σ) due to temperature and irreversible changes due to thermal coagulation. Two-compartment (tumor and healthy tissue) models were built and simulated. Reversible change of σ was modeled by a piecewise function characterized by increments of +1.5%/ºC up to 100 ºC, and a 100 times smaller value from 100 ºC onwards. Irreversible changes of σ were modeled using an Arrhenius model. We assumed that both tumor and healthy tissue had a different initial σ value (as suggested by the experimental data in the literature) and tended towards a common value as thermal damage progressed (necrotized tissue). We modeled a constant impedance protocol based on 90 V pulses voltage and three tumor diameters (2, 3 and 4 cm). Computer simulations showed that the differences between both models were only 0.1 and 0.2 cm for axial and transverse diameters, respectively, and this small difference was reflected in the similar temperature distributions computed by both models. In view of the available experimental data on changes of electrical conductivity in tumors and healthy tissue during heating, our results suggest that irreversible changes in electrical conductivity do not have a significant impact on coagulation zone size in two-compartment RFA models.

Keywords: electrical conductivity; irreversible changes; radiofrequency ablation; tumor ablation; two-compartment model

1. Introduction

Computer modeling has been widely used to study temperature distributions during radiofrequency (RF) tumor ablation (RFA). Up to now, this method involved solving an electrical-thermal coupled problem using a mathematical framework based on the Laplace equation to solve the electrical problem and the Pennes' equation for the thermal problem. The first computer models mimicked an RFA on non-tumor tissue, i.e. the tissue sub-domain was assumed to be homogeneous and constituted by a 'single compartment' [1–3]. Computer modeling was later used to explore temperature distributions in tumors with non-healthy tissue properties, for which two-compartment models were proposed: one compartment (or sub-domain) representing the tumor and the other the healthy tissue. Some two-compartment models considered a tumor with a cylindrical shape [4,5], while others assumed a spherical shape [6–8] or a two-layer setup [9]. About the RF applicator, some studies considered a multi-prong [6,7] while others modeled a single-needle RF applicator as the Cool-tip model [10–12].

The reason for two-compartment models was the experimental evidence that found that tumor electrical conductivity (σ) at RF frequencies is higher than that of healthy tissue. For instance, Haemmerich *et al* [13] measured σ at 1 MHz in *in vivo* tissues and reported mean values of 0.461 S/m for healthy liver and 0.523 S/m for tumor tissue. Prakash *et al* [14] reported mean values of 0.271 S/m for healthy *ex vivo* liver tissue and 0.471 S/m for tumor tissue (at 1 MHz). Haemmerich *et al* [15] reported mean values of 0.26 S/m for healthy liver and 0.504 S/m for tumor tissue (at 460 kHz) and Laufer *et al* [16] reported mean values of 0.15 S/m for healthy liver and 0.25 S/m for tumor tissue (at 400 kHz). This data hence suggested that RF power could be preferentially deposited in the tumor. In fact, the simulations conducted with two-compartment models showed more effective tumor destruction (in terms of temperature reached and coagulation zone volume) than those conducted with homogeneous (single compartment) models [10,11].

All the two-compartment models proposed to date have considered a change of σ exclusively dependent on temperature, based on an increase up to 100 ºC (e.g. +1.5%/ºC) and then a drop of several orders of magnitude to mimic the water loss associated with vaporization at this temperature (see Figure 1A) [4–7]. These models therefore did not consider irreversible changes of σ due to the accumulated thermal damage reported for non-tumor (i.e. healthy) tissues subjected to hyperthermic heating [17–20]. For instance, Pop *et al* [17] characterized the change of σ in *ex vivo* kidney at 460 kHz during and after heating at constant temperature (with target values between 48 and 78 ºC) and separated the changes in σ due to the reversible temperature effect (with a rate of +1.62%/ºC) from the permanent structural effect, which was modeled by an Arrhenius model. In general, they observed that in the samples heated to between 64.3 and 71.2 ºC, during cooling σ dropped to a higher value than for *native* tissue (as suggested by the orange line in Figure 1B). In this context, the adjective *native* refers to tissue that has not undergone heating, as opposed to *denatured*, which has been subjected to heating. Interestingly, Pop *et al* also reported 'aberrant' behavior in samples heated to 78.5 ºC, in which σ fell during cooling to a lesser value than samples heated to 71.2 ºC or lower (as suggested by the red line in Figure 1B). This behavior was associated with tissue desiccation, since the measurements were made after slow heating for several minutes.

Zurbuchen *et al* [18] measured σ at 470 kHz in *ex vivo* and *in vivo* liver samples subjected to heating and observed a plateau around 80 ºC (see green line in Figure 1C) and a return to the initial σ value after cooling (as suggested by the blue line in Figure 1C). Suspecting that the plateau was due

gradual tissue desiccation at slow heating, Macchi *et al* [19] measured σ at 480 kHz in *ex vivo* liver samples and compared changes in σ with temperature at fast and slow heating rates. They found that with fast heating the plateau disappeared and σ rose gradually to 100 ºC (maximum temperature used in their experiments), therefore returning almost to the starting point in Figure 1A (see black line in Figure 1D). These authors conducted RFA simulations considering different mathematical expressions to model the dependence of σ, ranging from those that only take temperature into account (as shown in Figure 1A) to those that included accumulated thermal damage at slow (Figure 1C) and fast (Figure 1D) heating rates. Interestingly, they did not find any large differences in terms of coagulation zone volume, although it should be remembered that they only simulated up to the first roll-off (impedance jump to 300 Ω). Macchi's study did not measure values of post-heating σ, i.e. during cooling. These results were later confirmed by Deas Yero *et al* [20], who measured σ at 500 kHz in *ex vivo* liver samples subjected to slow and fast heating.

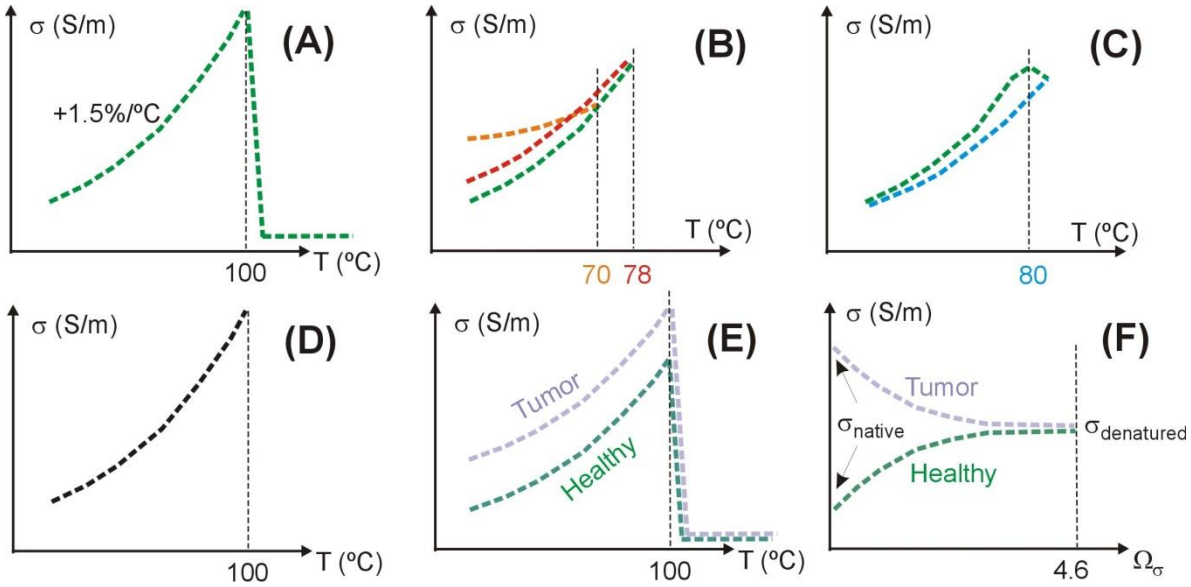

Figure 1. Overview of the proposed relationships between electrical conductivity (σ) and temperature (T) (see text for details) (A–D). Our modeling study seeks to compare the results obtained considering irreversible changes only (E) versus also considering irreversible changes, which means that the σ values of tumor and healthy tissue become more similar as ablation progresses, from σ_{native} (non-heated) to $\sigma_{denatured}$ (totally ablated).

If the studies on irreversible changes in σ with temperature in healthy tissues are not abundant, there is even less data on what occurs in tumor tissues. To our knowledge, only Haemmerich *et al* [15] reported σ values at 500 kHz in tumor tissue before and after ablation. Although these values were taken from a single patient, it is remarkable that while the healthy tissue σ was considerably lower than in the tumor before ablation (in agreement with other studies [13–16]), the difference between tumor and healthy tissue σ was greatly reduced after ablation. Although this finding may seem irrelevant, we think that it would be reasonable from a physical point of view to imagine that the difference in σ values of healthy tissue and tumor could be smaller after ablation because the two tissue types 'tend towards a similar physiological state', which is that of heat-induced necrotized tissue. If this were true, the advantage of tumor over surrounding healthy tissue in terms of improved

electrical conduction would not be sustained throughout several minutes of ablation, but would only exist before tumor ablation. Our goal was thus to explore how temperature distribution and coagulation zone size computed from a two-compartment model could vary in the case of including simultaneously reversible changes due to temperature, as suggested in Figure 1E, and irreversible changes due to thermal coagulation as suggested in Figure 1F (where σ could be modulated by an Arrhenius function Ω_σ, as previously done by Macchi *et al* [19] in case of homogeneous tissue) in the specific case of assuming that the differences in σ between healthy and tumor tissue disappear as tissue passes from *native* state to *denatured* state.

2. Materials and method

2.1. Modeling of tissue electrical conductivity

As in most two-compartment models, the electrical conductivities (σ) of healthy and tumor tissue were considered to be different, as has been reported in some experimental studies [13–16]. We used the values reported by Haemmerich *et al* [15]: 0.26 S/m for healthy liver and 0.504 S/m for tumor tissue (assumed to be taken at room temperature, 22 ºC).

The reversible change of σ associated with temperature was modeled using a piecewise function $\Phi(T)$ (as shown in Figure 1E) characterized by an increase of +1.5%/ºC until 100 ºC, followed by a reduction of two orders of magnitude between 100 and 101 ºC, and a constant value thereafter. This allows modeling the tissue desiccation associated with vaporization [19]. To sum up, the reversible change of σ with temperature was expressed as:

$$\sigma(T) = \sigma_{native} \cdot \ \Phi(T) \tag{1}$$

where σ_{native} is the electrical conductivity of healthy or tumor tissue at 22 ºC. On the other hand, the irreversible changes associated with the heating for each σ were modeled by assuming that both σ_{native} (tumor and healthy tissue) tend towards an identical value ($\sigma_{denatured}$) as the ablation progresses (as shown in Figure 1F). We assumed a $\sigma_{denatured}$ value equal to the mean value between the two σ_{native} i.e. 0.38 S/m (at 21ºC). To model the change from σ_{native} to $\sigma_{denatured}$ we used an Arrhenius model as proposed by Pop *et al* [17], which determines the first-order kinetic rate for the irreversible changes in electrical conductivity. The parameter Ω_σ represents the expected fraction of cells unaffected by irreversible changes, and is computed as follows:

$$\Omega_\sigma(T,t) = A_\sigma \int_0^t e^{-\frac{\Delta E_\sigma}{R \cdot T(\tau)}} d\tau \tag{2}$$

where A_σ is the frequency factor (6×10^{34} s^{-1}), ΔE_σ is the activation energy for the irreversible reaction (2.38×10^5 J/mol), R is the universal gas constant (8.314 J/mol·K) and $T(\tau)$ is the absolute temperature (K) as a function of time. The values of A_σ and ΔE_σ were taken from [17] and were those of *ex vivo* kidney tissue (none are available for liver). The parameter Ω_σ (associated with irreversible changes) was combined with Eq. 1 (associated with reversible changes) to obtain a full expression for changes of σ:

$$\sigma(T,\Omega_\sigma) = [\sigma_{native} + (\sigma_{denatured} - \sigma_{native}) \cdot (1 - e^{-\Omega_\sigma})] \cdot e^{0.015(T-T_{ref})} \tag{3}$$

where T_{ref} is the temperature at which the values of σ_{native} and $\sigma_{denatured}$ were considered (22 ºC). Figure 2 shows the change of σ with temperature (reversible changes) and Ω_σ (irreversible changes)

both for healthy and tumor tissues.

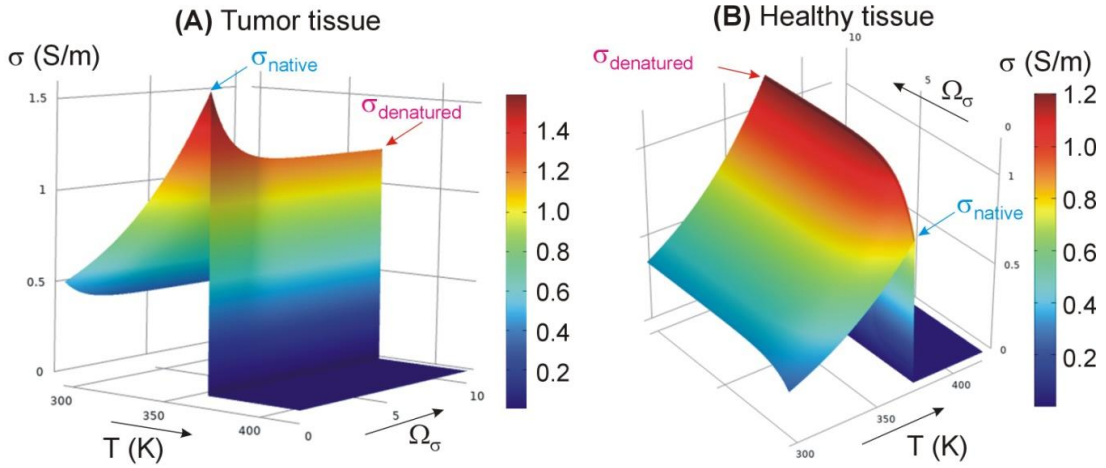

Figure 2. Change of σ with temperature (reversible changes) and Ω_σ (irreversible changes) both for tumor (A) and healthy (B) tissue.

2.2. Description of the model geometry

A two-compartment model was built and solved by the Finite Element Method using Comsol Multiphysics software (Burlington, MA, USA). The geometry of the problem was represented by a 2D axis symmetric model, which consisted of a cylindrical subdomain mimicking healthy liver tissue and a spherical subdomain mimicking tumor with different diameters (2, 3 and 4 cm) (see Figure 3). It also included a 3-cm 17G RF Cool-Tip applicator placed in the center of the tumor. The dispersive electrode was modeled as an electrical boundary condition V = 0 on all the outer boundaries except the symmetry axis. The internal cooling of the active electrode was modeled by setting a constant temperature of 10 ºC, while temperature was 37 ºC on all the outer boundaries except the symmetry axis. The model was based on a coupled electric-thermal problem in which the governing equation for thermal problem was the Bioheat Equation:

$$\rho c \frac{\partial T}{\partial t} = \nabla \cdot (k \cdot \nabla T) - \rho_b c_b \omega (T - T_b) + Q_m + Q_{RF} \qquad (4)$$

where ρ is tissue density, c tissue specific heat, T temperature, k tissue thermal conductivity, ρ_b blood density, c_b blood specific heat, T_b body temperature (37 ºC), ω blood perfusion coefficient (at temperature T_b), Q_m metabolic heat generation per unit volume (which can be negligible compared to other terms), and Q_{RF} heat source term due RF energy. Eq. (4) was applied to each region of the model by substitution of the appropriate properties. To calculate Q_{RF} we solved the electrical problem, which for RFA can be calculated by:

$$Q_{RF} = \vec{J} \cdot \vec{E} = \sigma \left|\vec{E}\right|^2 = \sigma |-\nabla V|^2 \qquad (5)$$

where $\vec{J}$ is the current density vector (A/m^2), $\vec{E}$ electrical field vector (V/m), σ electrical conductivity (S/m) and V voltage (V). We used quasi-static approximation to solve the electrical

problem where conduction currents were assumed to dominate compared to displacement currents. The electric voltage was computed by solving the equation [14]:

$$\nabla \cdot (\sigma \nabla V) = 0 \tag{6}$$

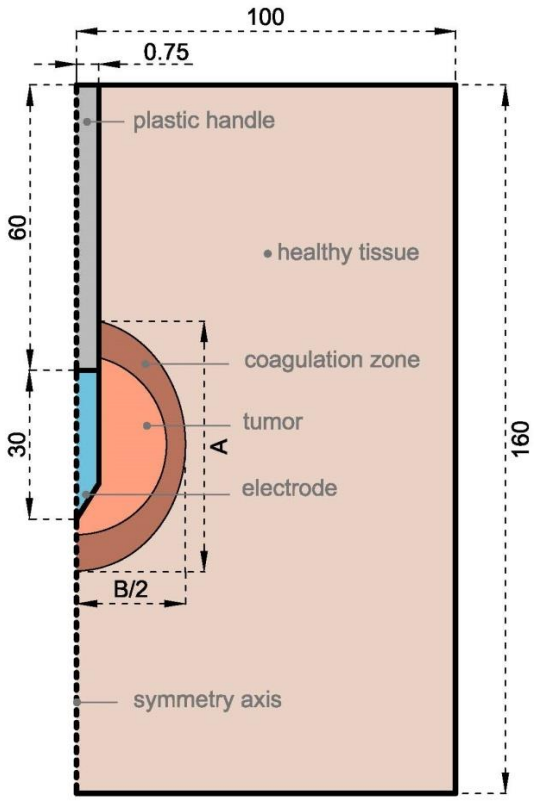

Figure 3. 2D axisymmetric model used to study the temperature distributions during RFA. It consisted of a cylinder of healthy liver tissue surrounding a spherical tumor of diameter varying between 2, 3 and 4 cm. The active electrode is inserted into the center of the tumor. A and B are the axial and transverse diameters, respectively (dimensions in mm).

Table 1. Characteristics of the materials used in the computational model [15,21].

Material	ρ **(kg/m^3)**	σ **(S/m)**	c **(J/kg·K)**	k **(W/m·K)**	ω **(1/s)**
Healthy tissue	1080	0.26	3455	0.502	0.016
Tumor	1045	0.504	3760	0.5	0.009
Blood	1046	-	3639	-	-
Metal (electrode)	8000	$7.4 \cdot 10^6$	480	18	-
Plastic (insulated trocar)	70	10^{-5}	1045	0.026	-

ρ: density, σ: electrical conductivity, c: specific heat, k: thermal conductivity, ω: blood perfusion. Tissue properties assessed at 37 °C (see text for more details related to σ thermal dependence).

Table 1 shows the values of the properties of the materials [15,21]. The accumulated thermal damage is the effect of exposing it to a high temperature for a prolonged time. A traditional way to predict the probability of irreversible thermal damage is the Arrhenius reaction rate model (as done in

Eq. (2)) in which the parameter Ω is related with the expected cellular survival fraction and is computed as follows:

$$\Omega(T,t) = A\int_0^t e^{-\frac{\Delta E}{R\cdot T(\tau)}}d\tau \qquad (7)$$

where A is the frequency factor ($7.39\cdot10^{39}$ s^{-1}), ΔE is the activation energy for the irreversible damage reaction ($2.557\cdot10^5$ J/mol), and R is the universal gas constant (8.314 J/mol·K). The parameters A and ΔE were taken from [10]. A value Ω = 4.6 (99% cell death probability) was used to compute the coagulation zone volume. Note that although Ω_σ and Ω have the same type of mathematical formulation (both are Arrhenius models), the former models the irreversible changes in tissue σ, while the latter models the vital state of the tissue.

We assumed that blood perfusion ceased once tissue was destroyed. This cessation was simulated by a first order kinetic model [7]:

$$\omega(T,t) = \omega_0 \cdot e^{-\Omega(T,t)} \qquad (8)$$

where ω_0 is the blood perfusion coefficient at temperature T_b.

In order to compare the two formulations (Eq. (1) vs. Eq. (3)), we conducted computer simulations with models: the one that considers only irreversible changes in σ (Model 1) vs. the one that also considers irreversible changes (Model 2). The computer simulations mimicked a controlled-impedance pulsed protocol as described in [22]. Basically, a constant voltage of 90 V is applied until the impedance exceeds a threshold of 100 Ω (roll-off). The voltage is then discontinued for 15 s, and the initial voltage value is reapplied. This is repeated every time a roll-off occurs for a total duration of 12 min, after which the computer simulates a 10 min cooling period in order to include the thermal latency and the subsequent enlargement of the coagulation zone [23]. The isoline Ω = 4.6 was used to compute the axial (A) and transverse (B) diameters of the coagulation zone (see Figure 3).

The models were verified in terms of mesh size, time-step and outer dimensions as described in [22]. The value of the maximum temperature reached in the tissue at the end of the ablation was used as a control parameter and a difference of less than 0.5% as a criterion between simulations.

3. Results

3.1. Verification of the model

Models 1 and 2 were verified in terms of spatial (mesh size) and time (time-step) discretization, along with the outer dimensions. Convergence tests were conducted to verify that the values used in the computer model represented the RFA with sufficient accuracy. The meshing size at the electrode-tissue interface was ~0.003 mm and at the point furthest from the active electrode was ~16 mm. The optimal time-step was ~0.5 s and the number of triangular elements ranged from 1300 to 1550, depending on the tumor size.

3.2. Effect of including irreversible changes of σ

Table 2 shows the axial and transverse diameters of the coagulation zone computed from the model considering only reversible changes of σ and from the model including also irreversible

changes. The differences between both models were 0.1 and 0.2 cm for axial and transverse diameters, respectively. This small difference between the results predicted by both models is also reflected in the marked similarity between the temperature distributions computed, as shown in Figure 4. There were hardly any differences between the number of roll-offs during RFA predicted by both models (29–32).

Table 2. Diameters of the coagulation zone computed from a model considering only reversible changes in σ (Model 1) and from the model also including irreversible changes (Model 2).

Tumor diameter	Axial diameter (cm)		Transverse diameter (cm)	
(cm)	Model 1	Model 2	Model 1	Model 2
2	5.0	5.1	3.6	3.4
3	5.2	5.3	3.7	3.5
4	5.0	5.1	3.4	3.6

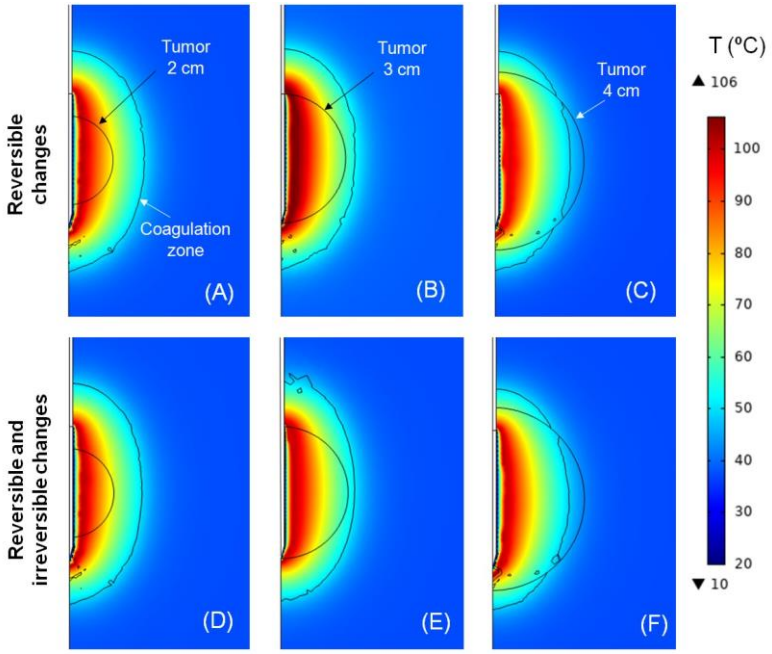

Figure 4. Temperature distributions computed after 12 minutes of RF ablation in tumors of 2, 3 and 4 cm diameter using two models with different changes of electrical conductivity during ablation: 1) reversible changes with temperature only (A–C), and 2) both reversible changes with temperature and irreversible changes associated with tissue denaturation (D–F). Coagulation zone limits corresponded with the isoline Ω = 4.6 computed from the Arrhenius model (Eq. (7)). Scale in ºC.

Due to the intricate mathematical formulation developed to model the reversible and irreversible changes in σ during RFA (see Eq (3) and Figure 2), it was crucial to check that each point of the domain (including tumor and healthy tissue) behaved as expected. In this regard, Figure 5 shows the evolution of the spatial distribution of σ at the beginning of the RFA (0 s), just after RF power application (720 s) and at two times during the cooling period following the cessation of RF power

(900 and 1320 s). As expected from a two-compartment model, at the initial time both models clearly show different σ values for the tumor and healthy tissue (see Figure 5A and 5 E). These are the values of tissue that has not undergone ablation, i.e. σ_{native}. In both models, a desiccated tissue area is clearly visible surrounding the electrode at the end of ablation (720 s). This is a narrow strip (blue in Figure 5B and Figure 5F), representing the extremely low values of reversible σ changes. Interestingly, at the same time, the model that only includes reversible changes (Figure 5B) is seen to keep a high σ value in the entire tumor sub-domain (red), while this does not occur in the model that also includes the irreversible changes (Figure 5F). During the cooling phase (i.e. when the RF power has been switched off), the σ values in healthy tissue and tumor are seen to return to their initial values in the reversible change-only model (see Figure 5C and 5D). The small differences just around the active electrode are due to the electrode cooling effect. However, in the model with irreversible changes it can be seen how the σ values in tumor and tissue tend to equalize in the areas affected by coagulation (they tend to value $\sigma_{denatured}$) and in fact they never return to their initial values (Figure 5G and 5H).

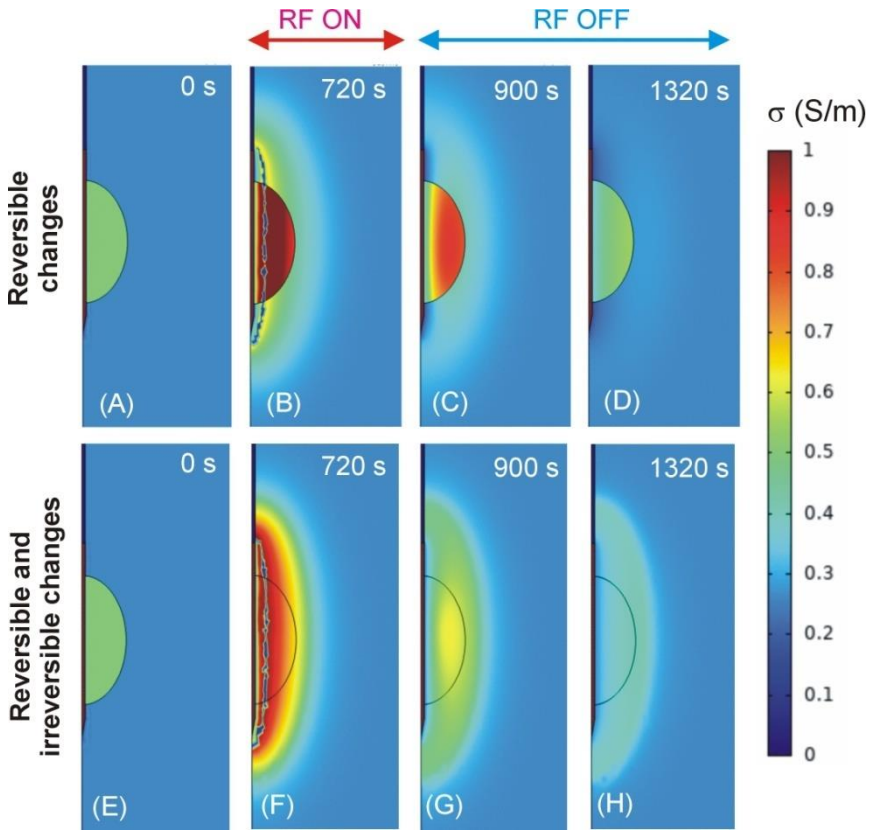

Figure 5. Spatial distributions of the electrical conductivity in tumor and healthy tissues before (t = 0 s), just after (t = 720 s) RFA and during the subsequent cooling period in which RF power is not applied (t = 900 and 1320 s). The plots are those of an RFA on a 2-cm tumor in two models with different changes of electrical conductivity during ablation: 1) reversible changes with temperature only (A–D), and 2) both reversible changes with temperature and irreversible changes associated with tissue denaturation (E–H). Scale in S/m.

4. Discussion

Despite the current absence of experimental data on the variations in σ values of healthy and tumor tissue during and after RF-induced heating, we proposed a new mathematical formulation to be included in two-compartment RFA models in order to include both reversible and irreversible changes in σ. Using the currently available values and assuming the difference between σ values of healthy and tumor tissue disappear as tissue passes from native state to denatured state (due to thermal coagulation) we conducted simulations to assess how a two-compartment model would predict coagulation zone volume when considering or ignoring irreversible σ changes. Our results show that after 12-minutes of RFA the results in terms of coagulation zone size are almost identical by both including and excluding irreversible changes. In other words, the coagulation zone size predicted by two-compartment RFA models is very similar if irreversible σ changes are either considered or ignored. This result is in agreement with that reported by Macchi *et al* [19], who found that the simulation results of constant power RFA on homogeneous tissue were almost identical for the different ways of modeling σ (both including and ignoring irreversible changes), although they argued that the Arrhenius-based model (which takes the irreversible changes into account) would be the most suitable since it automatically adjusts the σ value according to the thermal history. Our conclusions could obviously be different as new experimental values of σ become available for healthy and tumor tissue subjected to heating. Meanwhile, our contribution proposes a new model and checks its performance in a specific ablation case. The new formulation could also be applied to other models of other electromagnetic hyperthermic techniques focused on tumor ablation in which tissue electrical conductivity plays a relevant role [24], such as microwave ablation, or even to mathematical models based on other types of energy such as HIFU [25], since it is possible that other tissue characteristics (e.g. related with the fluid transport in the tissue [26,27]) have the same behavior as that hypothesized here for electrical conductivity, i.e. that normal and pathological tissue tend to have the same characteristics once coagulated.

Furthermore, the concept of a two-compartment model could be extended to ablation of other substrates (not just tumor), i.e. a generic model based on a central zone that mimics pathological tissue (target) and another surrounding zone that mimics healthy tissue, e.g. RF ablation of cardiac arrhythmias [28], in which the substrate causing the arrhythmia could be an area with differentiated electrical properties [29]. If we assume that the difference in σ values between healthy cardiac tissue and the ablation target (arrhythmogenic focus, post-infarct scar, etc.) will be smaller after ablation, the conclusions of the present study could have implication for more general two-compartment models. The concept of two-compartment model could also be applied to any RFA technique in which the target area has been doped with nanostructures [30–32]. Note that the properties of the zone 'seeded with nanostructures' could maintain different properties than the unseeded zones once both have been coagulated, in which case our conclusions would not be valid.

4.1. Limitations of the study

The study's main limitation is hence a certain amount of speculation in assuming that the σ values of tumor and healthy tissue will tend to equalize when they are subjected to RF-induced heating. In spite of this limitation, our contribution is to propose a novel mathematical formulation to model combinations of reversible and irreversible σ changes. The second limitation was using kidney data [17] to build the Arrhenius function (Eq. (2)) that modeled irreversible σ changes in both

healthy and tumor tissue (no liver or tumor data are currently available). The third is the lack of experimental validation for the proposed models, which is shared by all the two-compartment models proposed to date [4–12], due to the complexity of ablating tumor tissue under controlled conditions of size, position, electrical and thermal characteristics, etc. We also must recognize that the differences in coagulation zone size between models that include or ignore irreversible σ changes may not be so small under other ablation settings (duration, power).

Our two-compartment model took the differences in σ into account exclusively since it determines how electrical power is spatially deposited in the tissue. In fact, the development of a two-compartment model was motivated by the experimental evidence that tumor σ at RF frequencies is higher than that of healthy tissue, which suggests that targeting potency within the tumor would have a positive effect. However, we should point out that thermal properties (such as specific heat and thermal conductivity) could also show differences between tumor and healthy tissue and so could be included in future two-compartment models.

Finally, it is important to point out that our model was based on the Bioheat Equation. This equation assumes an infinite speed of heat transmission, which limits its use in some cases where large amounts of heat are applied to the tissues for very short times, as usually occurs in laser applications in which a change in the formulation is necessary, for example using the hyperbolic heat equation with a single or dual phase lag formulation. The time fractional approach has also been considered as an alternative formulation for heat transmission in tissues such as the cornea, which are also usually treated by laser. However, the RFA application conditions in the range of time and temperature gradients do not hinder the continued use of the Bioheat equation, so that the results do not change with these alternative formulations. Another assumption of the Bioheat Equation is that it assumes a uniform perfusion ratio and does not differentiate between blood and tissue, regardless of the direction of blood flow. A review of the models applied to hyperthermia treatments can be found in Andreozzi *et al* [33]. As there are currently no results that show a significant difference between the results obtained with the alternative models and those obtained with the Bioheat Equation, we here used the Bioheat Equation as the model.

5. Conclusion

This work analyzes the temperature distribution and coagulation zone size computed by a two-compartment radiofrequency ablation (RFA) model when including simultaneously reversible changes in the tissue electrical conductivity (σ) due to temperature and irreversible changes due to thermal coagulation. The computer simulations showed that the differences between both models were only 0.1 and 0.2 cm for axial and transverse diameters, respectively. This suggests that irreversible changes of electrical conductivity do not have a significant impact in terms of coagulation zone size on two-compartment RFA models, which means the mathematical framework of the two-compartment models for tumor RFA could be simplified.

Acknowledgments

This work was supported by the National Council of Science and Technology (CONACYT, México) through a scholarship grant to Dora Luz Castro-López, CVU registration Nº 446604; and by the Spanish *Ministerio de Ciencia, Innovación y Universidades* under "*Programa Estatal de I+D+i*

Orientada a los Retos de la Sociedad", Grant Nº "RTI2018-094357-B-C21".

Conflict of interest

The authors have no conflicts of interest or financial disclosures to make relevant to this submission.

References

1. D. Haemmerich, S. T. Staelin, S. Tungjitkusolmun, F. T. Lee Jr, D. M. Mahvi, J. G. Webster, Hepatic bipolar radio-frequency ablation between separated multiprong electrodes, *IEEE Trans. Biomed. Eng.*, **48** (2001), 1145–1152.
2. D. Haemmerich, L. Chachati, A. S. Wright, D. M. Mahvi, F. T. Lee Jr, J. G. Webster, Hepatic radiofrequency ablation with internally cooled probes: Effect of coolant temperature on lesion size, *IEEE Trans. Biomed. Eng.*, **50** (2003), 493–500.
3. I. A. Chang, U. D. Nguyen, Thermal modeling of lesion growth with radiofrequency ablation devices, *Biomed. Eng. Online*, **3** (2004), 27.
4. Z. Liu, S. M. Lobo, S. Humphries, C. Horkan, S. A. Solazzo, A. U. Hines-Peralta, et al., Radiofrequency tumor ablation: insight into improved efficacy using computer modeling, *AJR Am. J. Roentgenol.*, **184** (2005), 1347–1352.
5. S. M. Lobo, Z. J. Liu, N. C. Yu, S. Humphries, M. Ahmed, E. R. Cosman, et al., RF tumour ablation: computer simulation and mathematical modelling of the effects of electrical and thermal conductivity, *Int. J. Hyperth.*, **21** (2005), 199–213.
6. T. W. Sheu, C. W. Chou, S. F. Tsai, P. C. Liang, Three-dimensional analysis for radio-frequency ablation of liver tumor with blood perfusion effect, *Comput. Methods Biomech. Biomed. Eng.*, **8** (2005), 229–240.
7. D. Haemmerich, B. J. Wood, Hepatic radiofrequency ablation at low frequencies preferentially heats tumour tissue, *Int. J. Hyperth.*, **22** (2006), 563–574.
8. M. Ahmed, Z. Liu, S. Humphries, S. N. Goldberg, Computer modeling of the combined effects of perfusion, electrical conductivity, and thermal conductivity on tissue heating patterns in radiofrequency tumor ablation, *Int. J. Hyperth.*, **24** (2008), 577–588.
9. D. Haemmerich, D. J. Schutt, RF ablation at low frequencies for targeted tumor heating: In vitro and computational modeling results, *IEEE Trans. Biomed. Eng.*, **58** (2011), 404–410.
10. G. Zorbas, T. Samaras, Parametric study of radiofrequency ablation in the clinical practice with the use of two-compartment numerical models, *Electr. Biol. Med.*, **32** (2013), 236–243.
11. B. Zhang, M. A. Moser, E. M. Zhang, Y. Luo, H. Zhang, W. Zhang, Study of the relationship between the target tissue necrosis volume and the target tissue size in liver tumors using two-compartment finite element RFA modelling, *Int. J. Hyperth.*, **30** (2014), 593–602.
12. M. Jamil, E. Y. Ng, Quantification of the effect of electrical and thermal parameters on radiofrequency ablation for concentric tumor model of different sizes, *J. Therm. Biol.*, **51** (2015), 23–32.
13. D. Haemmerich, S. T. Staelin, J. Z. Tsai, S. Tungjitkusolmun, D. M. Mahvi, J. G. Webster, In vivo electrical conductivity of hepatic tumours, *Physiol. Meas.*, **24** (2003), 251–260.

14. S. Prakash, M. P. Karnes, E. K. Sequin, J. D. West, C. L. Hitchcock, S. D. Nichols, et al., Ex vivo electrical impedance measurements on excised hepatic tissue from human patients with metastatic colorectal cancer, *Physiol. Meas.*, **36** (2015), 315–328.
15. D. Haemmerich, D. J. Schutt, A. W. Wright, J. G. Webster, D. M. Mahvi, Electrical conductivity measurement of excised human metastatic liver tumors before and after thermal ablation, *Physiol. Meas.*, **30** (2009), 459–466.
16. S. Laufer, A. Ivorra, V. E. Reuter, B. Rubinsky, S. B. Solomon, Electrical impedance characterization of normal and cancerous human hepatic tissue, *Physiol. Meas.*, **31** (2010), 995–1009.
17. M. Pop, A. Molckovsky, L. Chin, M. C. Kolios, M. A. Jewett, M. D. Sherar, Changes in dielectric properties at 460 kHz of kidney and fat during heating: importance for radio-frequency thermal therapy, *Phys. Med. Biol.*, **48** (2003), 2509–2525.
18. U. Zurbuchen, C. Holmer, K. S. Lehmann, T. Stein, A. Roggan, C. Seifarth, et al., Determination of the temperature-dependent electric conductivity of liver tissue ex vivo and in vivo: Importance for therapy planning for the radiofrequency ablation of liver tumours, *Int. J. Hyperth.*, **26** (2010), 26–33.
19. E. G. Macchi, M. Gallati, G. Braschi, E. Persi, Dielectric properties of RF heated ex vivo porcine liver tissue at 480 kHz: measurements and simulations, *J. Phys. D Appl. Phys.*, **47** (2014), 485401.
20. D. D. Yero, F. G. Gonzalez, D. Van Troyen, G. A. E. Vandenbosch, Dielectric properties of ex vivo porcine liver tissue characterized at frequencies between 5 and 500 kHz when heated at different rates, *IEEE Trans. Biomed. Eng.*, **65** (2018), 2560–2568.
21. E. Ewertowska, R. Quesada, A. Radosevic, A. Andaluz, X. Moll, F. G. Arnas, et al., A clinically oriented computer model for radiofrequency ablation of hepatic tissue with internally cooled wet electrode, *Int. J. Hyperth.*, **35** (2019), 194–204.
22. M. Trujillo, J. Bon, M. J. Rivera, F. Burdio, E. Berjano, Computer modelling of an impedance-controlled pulsing protocol for RF tumour ablation with a cooled electrode, *Int. J. Hyperth.*, **32** (2016), 931–939.
23. R. M. Irastorza, M. Trujillo, E. Berjano, How coagulation zone size is underestimated in computer modeling of RF ablation by ignoring the cooling phase just after RF power is switched off, *Int. J. Numer. Method Biomed. Eng.*, **33** (2017), 10.1002/cnm.2869.
24. B. Zhang, M. A. Moser, E. M. Zhang, Y. Luo, W. Zhang, Numerical analysis of the relationship between the area of target tissue necrosis and the size of target tissue in liver tumours with pulsed radiofrequency ablation, *Int. J. Hyperth.*, **31** (2015), 715–725.
25. M. Mohammadpour, B. Firoozabadi, Numerical study of the effect of vascular bed on heat transfer during high intensity focused ultrasound (HIFU) ablation of the liver tumor, *J. Therm. Biol.*, **86** (2019),102431.
26. A. Andreozzi, M. Iasiello, P. A. Netti, A thermoporoelastic model for fluid transport in tumour tissues, *J. R Soc. Interf.*, **16** (2019), 20190030.
27. A. Andreozzi, M. Iasiello, P. A. Netti, Effects of pulsating heat source on interstitial fluid transport in tumour tissues, *J. R Soc. Interf.*, **17** (2020), 20200612.
28. M. Iasiello, A. Andreozzi, N. Bianco, K. Vafai, The porous media theory applied to radiofrequency catheter ablation, *Int. J. Numer. Methods Heat Fluid Flow*, **30** (2019), 2669–2681.

29. Y. Salazar, R. Bragos, O. Casas, J. Cinca, J. Rosell, Transmural versus nontransmural in situ electrical impedance spectrum for healthy, ischemic, and healed myocardium, *IEEE Trans. Biomed. Eng.*, **51** (2004), 1421–1427.
30. M. Qiu, A. Singh, D. Wang, J. Qu, M. Swihart, H. Zhang, P. N. Prasad, Biocompatible and biodegradable inorganic nanostructures for nanomedicine: Silicon and black phosphorus, *Nano Today*, **25** (2019), 135–155.
31. Z. Xie, T. Fan, J. An, W. Choi, Y. Duo, Y. Ge, et al., Emerging combination strategies with phototherapy in cancer nanomedicine, *Chem. Soc. Rev.*, 2020 Jun 22.
32. M. Luo, T. Fan, Y. Zhou, H. Zhang, L. Mei, 2D black phosphorus–based biomedical applications, *Adv. Funct. Mater.*, **29** (2019), 1808306.
33. A. Andreozzi, L. Brunese, M. Iasielllo, C. Tucci, G. P. Vanoli, Modeling heat transfer in tumors: A review of thermal therapies, *Ann. Biomed. Eng.*, **47** (2019), 676–693.